# JOURNAL OF SCIENCE

## PART A: ENGINEERING AND INNOVATION


**Year / Yıl: 2019** **Volume / Cilt: 6** **Issue / Sayı: 1**

**e-ISSN 2147-9542**

Gazi University

**Journal of Science**

PART A: ENGINEERING AND INNOVATION

http://dergipark.gov.tr/gujsa

Gazi University

**Journal of Science**

PART A: ENGINEERING AND INNOVATION

http://dergipark.gov.tr/gujsa

**Year / Yıl: 2019** **Volume / Cilt: 6** **Issue / Sayı: 1**

# CONTENTS

GU J Sci, Part A, 6(1): 1-8 (2019)

Gazi University

**Journal of Science**

PART A: ENGINEERING AND INNOVATION

http://dergipark.gov.tr/gujsa

# Aerodynamic Control in High Speed Trains with a Novel Design of Wing Set

Mehmet ÇİÇEK[1,*], Gökhan DURMUŞ[2]

[1]*Emek Mah. 2.Temel Sk. No 6 Hudeyfe Company, Antakya, Hatay, Turkey*
[2]*Faculty of Aeronautics and Astronautics, Anadolu University, Eskisehir, Turkey*

**ArticleInfo**

*Research Article*
*Received:12/09/2018*
*Accepted:24/12/2018*

**Keywords**

*High-speed trains (HSTs),*
*Aerodynamic breaking,*
*Aerodynamic control,*
*Railway,*
*Derail,*
*Wing,*
*Centrifugal force*

**Abstract**

Different from previous aerodynamic brake studies where aerodynamic brake is used to support conventional brakes, in this paper, a novel design of wing set for high speed trains (HSTs) has been proposed to provide safer and faster movement in curved rails. We have investigated, for the first time, the contribution of those two-axis wings on the running capability of a HST in a curved path to reduce derail or overturn risk. We have put 6 wings, 4 on sides which are proposed first time and 2 on top on each car. We have found that at same speed (0.8ma), minimum radius of curvature decreased from 7km to 3km when the wings are used. In the second part, the advantages of the aerodynamic drag brakes induced from proposed novel design wings at the speed of 0.8ma are discussed.

## 1. INTRODUCTION

In the 19th century the speed of the trains was about 100 km / h. It was utopia that the speed of the trains reached 250 km / h in those days. Newly, high-speed trains (HSTs) can get speeds of up to 400 km/h and test trains reaching 600 km/h have been produced [Zhang et al. 2018, Jianyong et al. 2013]. HSTs have become a popular and important transportation way due to its advantages of high speed and efficiency, which draws attention worldwide [Li et al. 2017]. As it will be appreciated, the increase in velocity increases the attention worldwide and importance of aerodynamic controlling of a HST.

In connection with the increasing speed, many engineering problems, which have been ignored at low speeds, come up [Vasovic et al. 2011]. When driving fast on a straight path, the vehicle should have a minimal aerodynamic drag, and the down force does not need to be large. When braking, the vehicle should have a significant aerodynamic drag and should produce a greater down force [Pietrzak P. and Piechna J., 2013]. The fast cornering and driving through curves requires great aerodynamic down force and the forces acting perpendicular to the wheels on both side must be close to each other. The actuatable aerodynamic parts (wings) attached to the vehicle body can be the solution that change the aerodynamic characteristics of the vehicle and minimize derail or overturn risk. Therefore, actuatable wings should be used not only in braking but also be used in such cases like secure fast cornering.

The force equivalent of the HST braking force is proportional to the square of the velocity. Thus, aerodynamic brake method is very effective at high speeds [Wu et al. 2011]. Unlike sliding frictional shoe brake and wheel disc brake, the aerodynamic brake is designed to produce negative force by increasing aerodynamic drag with wings or panels attached to the car body [Yoshimura et al. 2000]. In aerodynamic brake, wings block the air stream and a positive pressure occurs in front of it while negative pressure is formed behind it. The resulting pressure difference creates a resistance force normal to the surface of the panel and serves as a braking force. When a HST enters to a curved path, different magnitudes of forces

*Correspondingauthor, e-mail:elektrik.mehmetcicek@gmail.com

are applied to the left and right wheels. If there is a large difference between the magnitudes of forces, the HST may derail or overturn. But independent-controlled two axis-wings attached to the cars of a HST can be used to equalize the forces on wheels on both sides to ensure safer and faster travel.

In this study, I proposed a novel design of wing set attached to the cars of a HST and have investigated, for the first time, the effects of those two-axis wings on the running capability of a HST in a curved path to reduce derail or overturn risk. In the second part, the contributions of aerodynamic drag brakes induced from novel design wings are examined. It is assumed that the HST has five cars (Fig. 1).

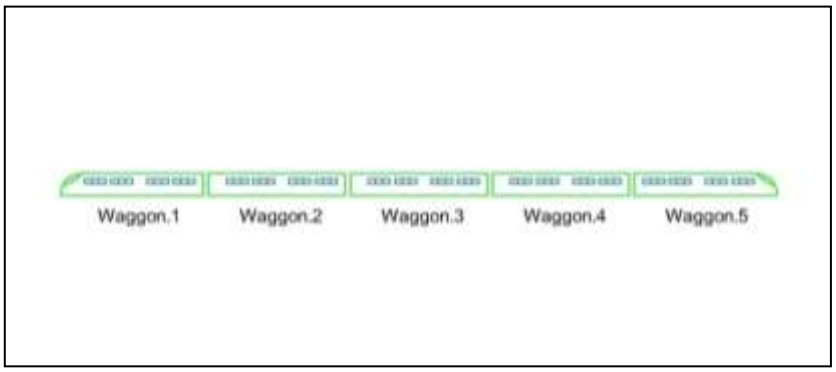


***Figure 1.*** *Schematic drawing of a high speed test train*

Each car's length, width and height are 25m, 4m and 4m, respectively (Fig. 2). Each car has 6 unibody wings, two on top and four on sides which are reversely movable (Fig. 3).

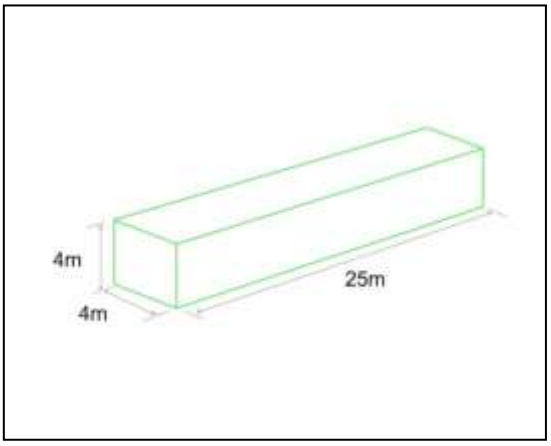


***Figure 2.*** *Assumed dimensions of each car*

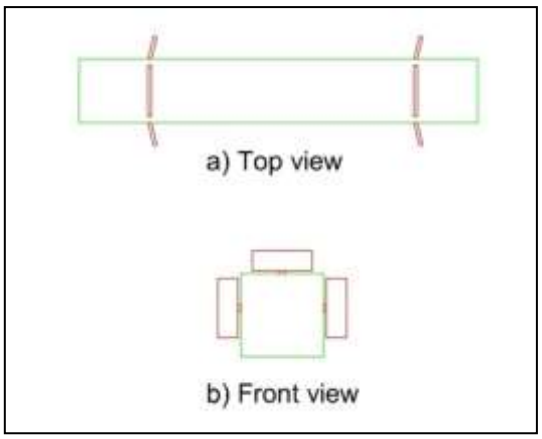


***Figure 3.*** *Placements of the wings on a single car*

The train speed was considered as to be 0.8 ma. All wings are actuatable and can move independently in two dimensions around z and y axis (Fig. 4).

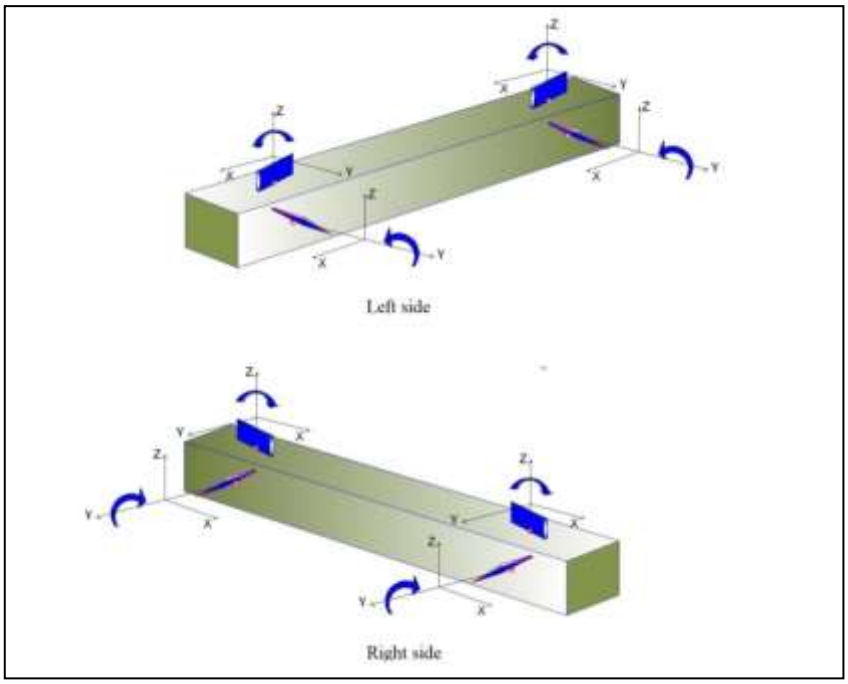


***Figure 4.*** *Actuatable wings which can be controlled independently in two dimensions around z and y axis*

They are normally closed when the train moves straight. The wings of course act as aerodynamic drag brake for slowing the vehicle in addition to conventional brake. But we primarily aim to use these two axis-wings for ensuring safer travel in curved paths by modifying the forces acting on $P_1$and $P_2$wheels (Fig. 5). When the angular positions of the wings are changed, forces on $P_1$and $P_2$can be tuned accordingly.

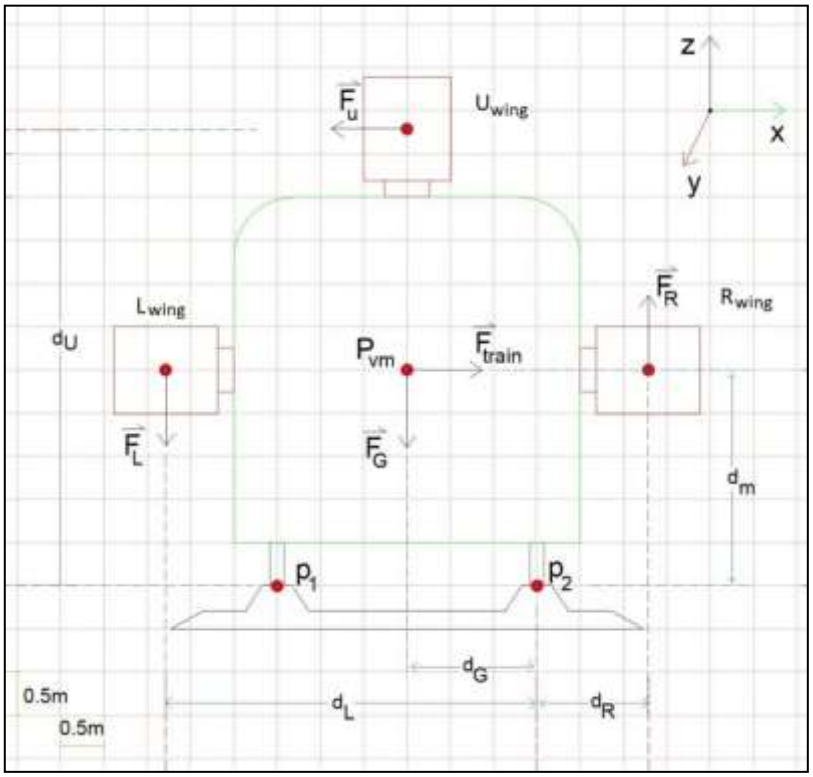


***Figure 5.*** *Front view of a car showing the forces acting on the wheels*

## 2. MATERIALS AND METHODS

### 2.1. Aerodynamic Control

The magnitude of centrifugal force ($F_{train}$) and its moment according to the points $P_1$and $P_2$can be estimated by using the following equations, respectively [Halliday and Resnick, 1981];

$$F_{train} = mV^2/r \quad (1)$$
$$M_{train} = d_m F_{train} \quad (2)$$

where m is the mass of car, $V$ is linear velocity, $r$ is radius of curvature (Fig. 6) and $d_m$ is the perpendicular distance of the force to the points $P_1$ or $P_2$. The moment that the wings generate ($M_{wing}$) causes overturning moment of $F_{train}$ to decrease. (Fig. 7).

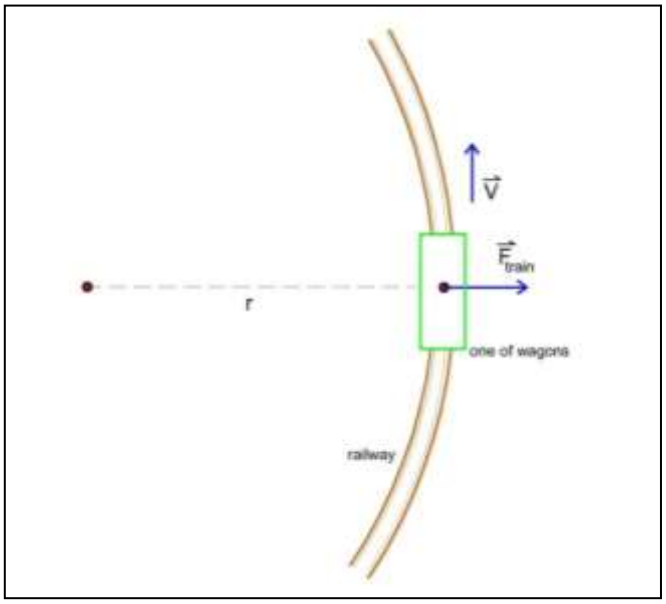


***Figure 6.*** *Schematic description of radius of curvature*

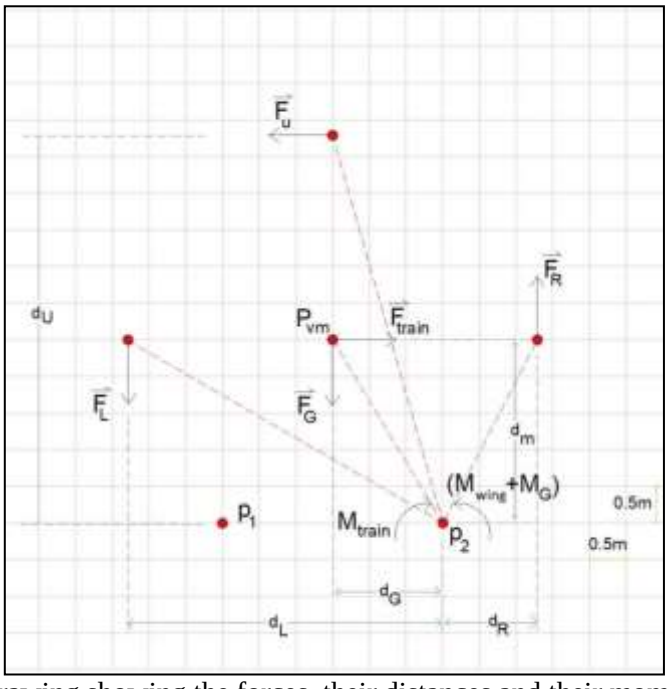


**Figure 7.** A schematic drawing showing the forces, their distances and their moments

The total moment and the forces caused by the upper, left and right wings for a single car can be estimated by performing the following calculations;

$$M_{total} = M_{train} + M_{wing} + M_G \quad (3)$$
$$M_{total} = d_m F_{train} + 2F_U d_U + 2F_R d_R + 2F_L d_L + d_G F_G \quad (4)$$
$$F_L = F_U = F_R = \frac{1}{2}\rho_0 V^2 S C_L \quad (5)$$
$$F_G = mg \quad (6)$$

where $M_G$is the moment of gravity of the car, $\rho_0$is the density of air, $S$ is surface area of each wing, $C_L$ is the lift coefficient, $g$ is the acceleration of gravity and $F_U F_R$ and $F_L$ are the forces caused by upper, right and left wings, respectively. In Equation 5, the value of $C_L$ will change according to the angel of wing. This work was considered as a wing NACA0012. The $C_L$ value varies from 0.1 to 1.4. It was considered as 0.5 in the current study.

By performing a sample numerical analysis, we can see the effect of the wings. The preferred values for calculation are shown in Table 1.

***Table 1***. *The preferred values for calculation of aerodynamic control*

| **The values used in the calculation** | | | |
|---|---|---|---|
| ***r* (m)** | **$d_U$ (m)** | **$d_R$ (m)** | **$d_L$ (m)** |
| 20000 | 5.3 | 1.3 | 4.3 |
| **$d_m$ (m)** | **$C_L$** | **$S$ (m$^2$)** | ***m* (kg)** |
| 2 | 0.5 | 3 | 60000 |
| **$g$ (m/s$^2$)** | **$\rho_o$ (kg/m$^3$)** | **$d_G$ (m)** | ***V* (ma)** |
| 9.8 | 1.225 | 1.5 | 0.8 |
| **Calculated values** | | | |
| **$F_{train}$** | 165.675 kN | **$M_U$** | 537.8224 kNm |
| **$M_G$** | 882.000 kNm | **$M_L$** | 436.3465 kNm |
| **$F_U$= $F_L$=$F_R$** | 50.7379 kN | **$M_R$** | 131.9187 kNm |
| **$M_{train}$** | 313.350 kNm | **$M_{flap}$** | 1106.087 kNm |

As can be seen from the Table 1, the moment caused by the wings is 3.5 times much larger than that of centrifugal force. It means that the train can safely run at a speed of 0.8ma on a curved rail with a radius of curvature of 20km.

In case in which the wings are closed, due to the mass of the train (Fig. 8), at the speed of 0.8 ma, the minimum radius of curvature of the rail required for the train to travel without overturning or derailing is 7 km. But, when the wings are used, the train can travel safely on a curved path with a radius of curvature of 3km if the weight of the train taken into account.

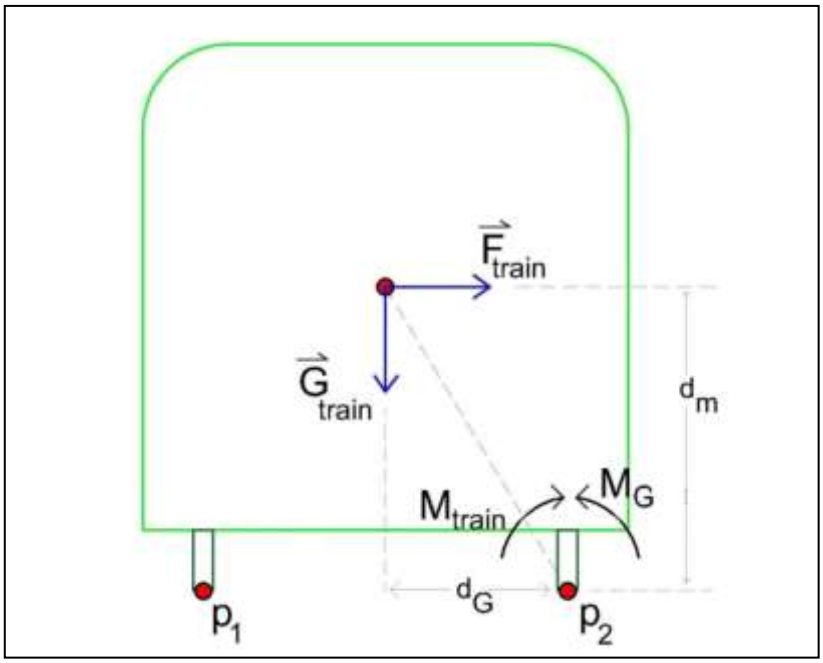


***Figure 8.*** *A schematic drawing showing the moments induced from the mass of train and the centrifugal force*

### 1.2. Aerodynamic Breaking

In HSTs, the braking systems can be classified as adhesion braking and non-adhesion braking. In adhesion braking, the maximum force between the wheel set and the rail limits the braking force while this limitation does not exist in non-adhesion braking [Sharma et al. 2015]. Therefore, non-adhesion braking techniques such as aerodynamic braking, eddy current braking and electromagnetic rail braking have great attention as techniques at high speeds to overcome the problem of effective braking [Vasovic et al. 2011; Jianyong et al. 2013]. Aerodynamic braking has several advantages over non-adhesion braking methods i) It stretches the brake panel to enhance aerodynamic resistance when braking. Since aerodynamic resistance is proportional to the square of the relative velocity, aerodynamic braking performs efficiently at high speed, and can be used to compensate for the deficiencies of adhesion braking. ii) Aerodynamic braking uses the relative speed between the natural wind and the vehicle. Unlike other braking methods, such as disc braking and electrical braking, aerodynamic braking has a relatively simple control scheme [Jianyong et al. 2013].

When the aerodynamic brake is in the extended position, it blocks the airflow and overpressure occurs in front of it, while behind it an area of negative pressure is formed due to the flow separation behind the plate. The difference in pressures between the front and the rear brake panel surface creates a resistance force normal to the surface of the panel and serves as a braking force. The tangential force induced by the surface friction is negligible when compared to the normal force [Vasovic et al. 2011].

In this section, the influence of the wings which are perpendicular to airflow is examined. All wings were taken into account to calculate total braking effect of them. The friction forces and viscous forces are neglected. A simple Matlab algorithm can be used to calculate the effect of wings. The following equations were used to calculate drag force, acceleration and final velocity, respectively. Table 2 shows the values chosen just for example and calculated quantities. Because drag coefficient ($C_D$) changes between 0.03 and 1.4, it has been taken as 0.5 that is an average value.

$$F_{drag} = \tfrac{1}{2}\rho_0 V^2 S C_D \quad (7)$$

$$a = F_{drag}/m \quad (8)$$

$$V_{final} = V_{initial} - at \quad (9)$$

***Table 2.*** *The values used in the calculation and the estimated final speed*

| $V_{inital}$ (km/h) | $\rho_o$ (kg/m$^3$) | $C_d$ - | $m$ (kg) | $S$ (m$^2$) | $t$ (s) |
|---|---|---|---|---|---|
| 1000 | 1.225 | 0.5 | 300000 | 90 | 90 |
| Calculated final speed (km/h) | | | | | |
| $V_{final}$=269 | | | | | |

As can be seen from the Table 2, train speed decrease from 0.80ma to about 0.22ma after 90 seconds of aerodynamic braking without the help of any other braking system under our experimental conditions. When the train speed falls below 300 km/h, it can be switched to conventional braking. Aerodynamic braking and conventional braking can be used together in emergency situations.

## 3. CONCLUSION

Aerodynamic control in high-speed trains will be an important study area for the future. In this study, we proposed a novel design wing set attached to both side and top of the car for the first time. We investigated the advantages of the wings on reducing derail or overturn risk. It was found that minimum radius of curvature decreased from 7km to 3km with the usage of wings. With the support of the proposed wing set, it was estimated that, the train having the speed of 0.80ma decreased its speed to 0.22ma after 90 seconds of aerodynamic braking without the help of any other braking system. The results of the analysis showed that aerodynamic control has serious advantages.

- Reduces the risk of centrifugal force and derailment risk, ensuring that the train travels more safely,
- It can ensure that the train keeps its speed during cornering,
- It shortens the travel time,
- It extends the life of the wheel bandages.
- It extends the life of electric motors by reducing dynamic braking.
- It reduces the wear of the railway.

This work keeps a light on the work that will enable fast trains to travel at very high speeds. Patent assessment of this wing design proposed in the paper is pending.

## CONFLICT OF INTEREST

No conflict of interest was declared by the authors

## REFERENCES

Halliday, R., Resnick, R., 1981. Fundamentals of physics, 2nd edition, *John Wiley & Sons*, New Jersey.

Jianyong, Z., Mengling, W., Chun, T., Ying, X., Zhuojun, L., Zhongkai, C., 2013. Aerodynamic braking device for high-speed trains: Design, simulation and experiment. *Proceedings of the Institution of Mechanical Engineers, Part F: Journal of Rail and Rapid Transit* 228: 260.

Li, Z., Yang, M., Huang, S., Liang, X., 2017.A new method to measure the aerodynamic drag of high-speed trains passing through tunnels.*Journal of Wind Engineering & Industrial Aerodynamics* 171: 110–120.

Pietrzak P., Piechna J., 2013. Numerical investigation of the controllable wing stall caused by the air injection, *The Archive of Mechanical Engineering*, LX(2): 199-216.

Sharma, R.C., Dhingra, M., Pathak, R.K., 2015.*Braking Systems in Railway Vehicles. International Journal of Engineering Research & Technology*, 4(1): 206-211.

Vasović, I., Maksimović, M., Puharić, M., Matić, D., Linić, S., 2011.*Structural Analysis of Aerodynamic Brakes in High-Speed. Trains Scientific Technical Review*, 61(2): 10-15.

Wu, M., Zhu, Y., Tian, C., Fei, W., 2011. Influence of aerodynamic braking on the pressure wave of a crossing high-speed train. *Journal of Zhejiang University-Science A (Appl Physics & Engineering)* 12(12):979-984.

Yoshimura, M., Saito, S., Hosaka, S., Tsunoda, H., 2000.Characteristics of the Aerodynamic Brake of the Vehicle on the Yamanashi Maglev Test Line.*Quarterly report of Railway Technical Research Institute*, 41(2): 74-78.

Zhang, J., Wang, J., Wang, Q., Xiong, X., Gao, G., 2018. A study of the influence of bogie cut outs' angles on the aerodynamic performance of a high-speed train.*Journal of Wind Engineering & Industrial Aerodynamics* 175: 153–168.

GU J Sci, Part A, 6(1): 9-24 (2019)

Gazi University

**Journal of Science**

PART A: ENGINEERING AND INNOVATION

http://dergipark.gov.tr/gujsa

# Investigation of Thermal History and Optimization of Thermal Stresses in Friction Stir Welded Copper Sheets

Alireza ASGHARI[1], Reza POURHAMID[2,*], Ali SHIRAZI[3]

[1,2] *Department of Mechanical Engineering, Islamic Azad University, Shahr-e-Qods Branch, Tehran, Iran*
[3] *Department of Mechanical Engineering, Qom University of Technology, Qom, Iran*

**Article Info**

*Research Article*
*Received: 12/11/2018*
*Accepted: 25/03/2019*

**Keywords**

*Friction stir welding,*
*Thermal history,*
*Taguchi method,*
*Finite elements,*
*Frigaad relation*

**Abstract**

In the present study, thermal history have been determined for joined copper sheets under various welding conditions using Frigaad relation, numerically. The obtained results were compared with the experimental results and it was found that there is a good agreement between them. Also, it was found that the traverse velocity mainly affects the amount of transferred heat and the rotational speed changes the temperature of the welding process. This study cleared that in all welding conditions at first, the thermal history diagrams predicted using Frigaad relation are lower than the diagrams obtained from the experiments and then, the trend of process diagrams reverses and the simulation diagrams place higher than the experiment diagrams. In addition, Signal-to-noise analysis shows that shoulder diameter is a significant factor and plays a major role in affecting the longitudinal tensile thermal stresses.

## 1. INTRODUCTION

Friction stir welding is one of the new methods of connecting components to each other that compared to other methods is a relatively new one. This method was originally invented for connecting aluminum parts but its use was quickly extended to other materials such as magnesium, copper, steel, titanium, zinc [1] and many polymeric [2] and thermoplastic [3] materials. It was used to connect pieces with different materials as well [4-6]. This method was invented and introduced by The Welding Institute (TWI) in England in 1991 [7]. Recently, by developing the application of copper and its alloys as a structural material, the demand for the use of the method for welding the material is growing [8, 9]. Accordingly, copper has been chosen for the present study. Copper is applied to build pipes and ducts in many industries [10] and due to the corrosion resistance in plumbing [11, 12]. It is also used for water supply at homes [13] in the way that in the world, 80% of water supply systems are made of copper [14].

One of the important issues in FSW is to determine the thermal history and distribution in workpiece during the welding process [15]. This issue is important from two points: first, it can be determined whether welding is possible or not in a particular condition and Second, the thermal history and distribution in a piece affect the residual stress and grain size, thus it affects the weld strength [15]. Hence, a lot of researchers have attempted to provide experimental strategies or analytical models to determine thermal distribution in the workpiece. For example, Hwang et al. could specify the thermal history in the specific parts of workpiece through placing thermometers in aluminum sheets and welding them applying the mentioned method [15]. Also, Xue et al. were able to evaluate the thermal effect on the mechanical properties of obtained welds via FSW on copper in water and air and with different temperatures and determining the maximum temperature [16]. Imam et al. compared the relationship between mechanical and microstructural properties of stir areas and affected by temperature with maximum temperature for aluminum alloys [17].

*Corresponding author, e-mail: rpourhamid@gmail.com

Along with the conducted analytical and experimental studies, some researchers used numerical methods for determining the field of thermal distribution and its history in some parts of workpieces. For instance, using DEFORM-3D software, Buffa et al. could specify the thermal field in two parts of AA6060-T4 aluminum pieces connected by FSW [18]. Also, using Euler model, Jacquin et al. determined the thermal history and distribution in AA6060-T4 aluminum sheets and compared them with values obtained from the test [19]. Al-Badour et al. achieved the values of maximum temperature in FSW of AL6061-T6 aluminum through presenting Eulerian – Lagrangian model and compared them with experimental values [20].

Javadi et al. optimized residual stresses produced by friction stir welding of 5086 aluminum plates using Taguchi method. They optimized parameters including feed rate, rotational speed and pin diameter [21]. Also, Ugender studied the effect of friction stir welding parameters such as tool pin profiles, rotational speed and welding speed on the mechanical properties of tensile strength, hardness and impact energy of magnesium alloy AZ31 [22]. In this investigation, the experiments were carried out as per Taguchi parametric design concepts and an $L_9$ orthogonal array. He found that the important parameters influencing the weld mechanical properties are tool pin profiles and the combination of rotational speed and welding speed.

In the present study, two copper pieces have been welded together by the friction stir welding method under different welding conditions. The thermal history has experimentally been determined in a specific point of these pieces too. Then, using a numerical method and an empirical relation, the thermal history has been determined at the same points and under the same circumstances and has been compared with experimental results. Finally, three important process parameters including tool rotational and traverse speed and shoulder diameter have been optimized using Taguchi method.

## 2. MATERIALS AND METHODS

To carry out the tests, copper samples with lengths of 135 mm and widths of 50 mm were cut perpendicular to the rolling direction from a large sheet with a thickness of 5 mm. The content of the constituent elements of copper used in this study based on quantitative tests is presented in Table 1.

***Table 1.*** *The weight percentage of constituent elements of copper used in the study*

| Cu | Pb | Sn | P | Ni | Ag | Zn |
|---|---|---|---|---|---|---|
| Base Metal (99.86) | 0.005 | 0.0041 | 0.0224 | 0.0011 | 0.0017 | 0.0092 |

After smoothing the intended sections, the samples were placed together in a die for the welding process and were fixed towards each other by the die constraints. In addition to keeping the two workpieces fixed towards each other, the die constraints pushed them to the bottom of the die, where a copper plate is embedded. This copper plate at the bottom of the die is responsible for cooling the workpieces. As can be seen in Figure 1, the water enters the die via a hose and flows under the copper plate and into the slots, which are created under the copper plate for this purpose. This has a cooling effect on the copper plate of the die. Also, the copper plate, which is in direct contact with the workpieces, serves to transfer heat from the workpiece to the water, thereby reducing the temperature of the workpieces.

After cooling, the water flow enters into the exit hose from the other side of the die and exists through it. The mass rate of water passing through the die is equal to 0.019 kg/s. Cooling is done to transfer rapidly heat from pieces so that the opportunity of grain growth is taken from their microstructures. In many studies and references, it has been acknowledged that within the FSW process, cooling and removing rapidly heat from pieces lead to improving the properties of most materials [23-25].

A rotary tool used for doing the FSW process includes a shoulder with a diameter of 20 mm and a pin with a diameter of 8 mm and length of 4.7 mm. In order to improve the material travels, some threads are created on the pin which lets the material moves better around the instrument and to some extent it will move the axis. The tilt angle is considered as 2.5 degrees on the instrument. The indentation of the shoulder in the pieces (Plunging) is also 0.2 mm.

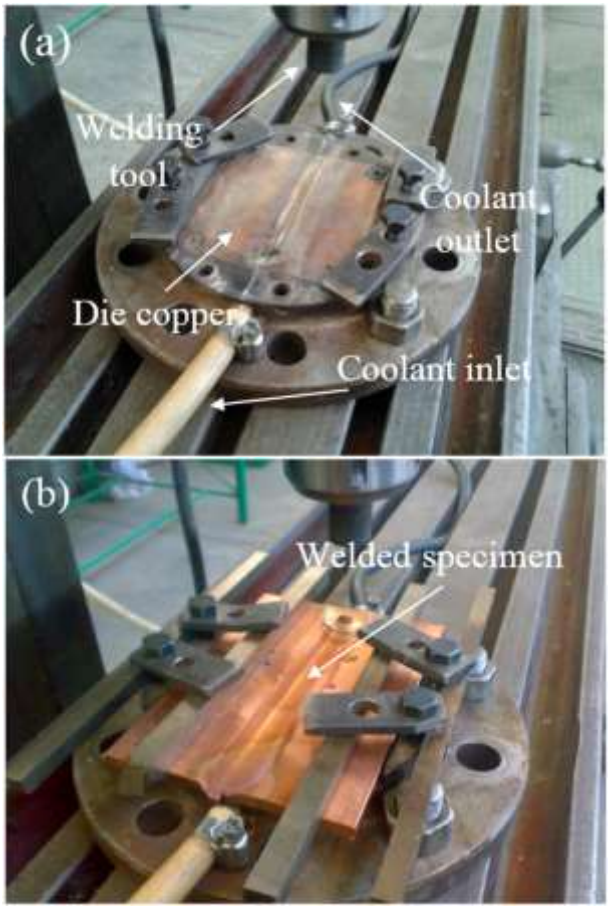


***Figure 1.*** *View of (a) the tools and the die used in the welding process and (b) the pieces fixed to the die after the welding process.*

The appropriate welding conditions for successful welding of the mentioned samples were determined by welding under different conditions (presented in Table 2) and using a trial and error method. Also, the point whose temperature has experimentally and numerically been measured for each welding cases has been indicated in Figure 2.

***Table 2.*** *Different cases used in welding.*

| Investigated cases | Rotational speed, N (rpm) | Traverse speed, v (mm/min) |
|---|---|---|
| Welding conditions 1 | 500 | 56 |
| Welding conditions 2 | 500 | 112 |
| Welding conditions 3 | 710 | 56 |

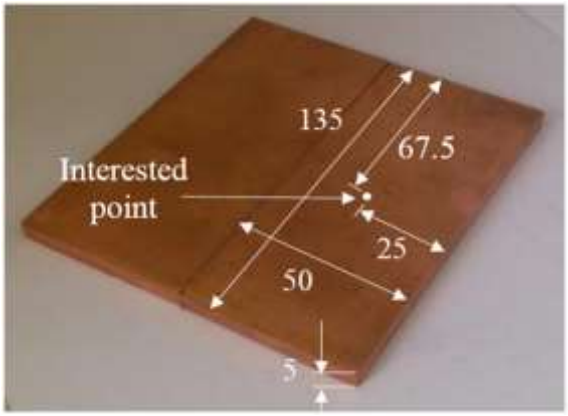


***Figure 2.*** *The point whose temperature has experimentally and numerically been measured for each welding cases.*

An infrared thermometer was used to measure the temperature in the workpiece. The thermometer was fixed on the table of a milling machine and moves with it (Figure 3). The thermometer reads the temperature values for a particular point at any time and instantaneously sends the obtained information to a manual computer to record via a receiver. So, by focusing the thermometer on the specific point of the surface of the workpiece, in the advancing side, its thermal history can be recorded instantaneously on the computer. This particular point is the midpoint of one of the two sheets that should be welded together (Figure 2).


***Figure 3.*** *Thermometer installed on the table of angle grinder for measuring instantaneous temperature.*

In order to determine the stress-strain diagram for the base metal at various temperatures, the standard samples of the tensile test were prepared based on ASTM-E8 standards shown in Figure 4(a) [26]. Also, Figure 4(b) shows the electric furnace used for high-temperature tensile tests. The true stress-strain diagram from the tensile test was obtained at two temperatures of 700°K and 800°K. These temperatures were chosen because they were approximately maximum temperatures that workpieces experienced on the conditions mentioned in Table 2. These temperatures were measured by infrared thermometer exclusively behind the tool in each welding mode during welding processes. Figure 5 shows true stress-strain diagrams of the base metal at two temperatures of 700°K and 800°K.

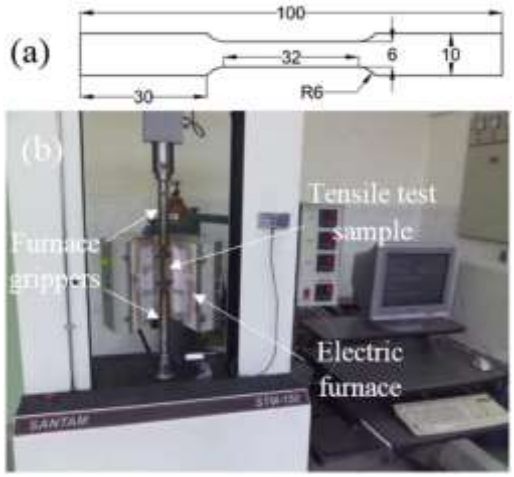


***Figure 4.*** *(a) Tensile test sample dimensions (in mm) (b) Electric furnace used for high temperature tensile tests.*

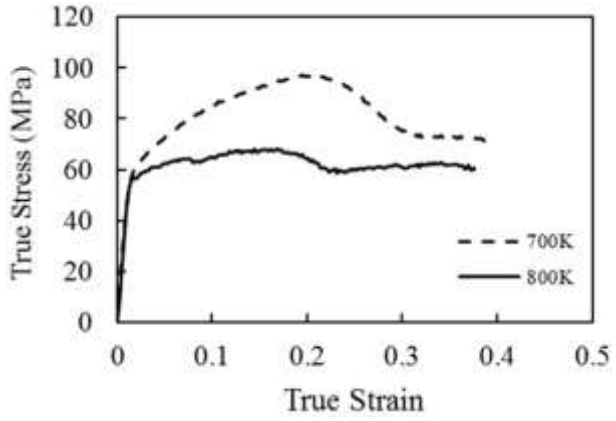


***Figure 5.*** *True stress – strain diagram of the base metal at two temperatures of 700°K and 800°K.*

## 3. SIMULATIONS

In order to simulate and determine the thermal field numerically in the workpiece, LS-Dyna software was used. For modeling the process of welding in the software, the option of thermal weld was used. This option was particularly included to simulate the process of welding in the mentioned software. Using this option, the rotary tool that is the thermal generator in the process of friction stir can be modeled as a heat source and moved along the surface of the workpiece with the desired speed. By moving this heat source on the workpiece, the heat can transfer to the workpiece and the temperature of the workpiece can increases at various parts of the workpiece, based on the heat transfer rate. To determine the produced heat rate by the rotary tool, within the process of friction stir welding, several relations are presented in various references. One of the important relations is the one provided by Frigadd et al. [27] that is used for calculating the heat generated by the tool. This relation is as follows:

$$\dot{q}=\frac{4}{3}\pi^2\mu P\omega R^3 \tag{1}$$

Where $\dot{q}$, $\mu$, P, $\omega$ and R are the rate of net heat input (W), the coefficient of dynamic friction, pressure (Pa), the angular speed (rps) and tool radius (m), respectively. According to Frigadd theorem, the rotational speed of tool and its radius have the most effect in generated heat. Also, Frigadd et al. suggested that the P be considered equal to flow stress at the temperature of the process [27].

In the present study, to obtain the rate of produced net heat, the above relation has been used. In so doing, the dynamic friction coefficient between tool and workpiece has been considered equal to 0.36 [28]. P-Value is equal to the flow stress of the material of workpiece at the temperature at which the process is performed. As we know, the flow stress is the stress in which deformations are of a plastic type. Given Figure 5, it can be found that after crossing from the yield stress and entering to the flow stress area, the true stress-strain diagram of copper at high temperature become first ascending and then descending and thereafter, it will be horizontally and fairly constant. Therefore, given that for using Equation 1 and obtaining the rate of produced heat at the certain temperature and a specified rotation of tool (N), a constant number should be used and this number i.e. the flow stress of workpiece material has been considered in the temperature of the process equal to the stress of horizontal area of the diagram. Thus, P was considered at the temperature of 700 °K equal to 72MPa and 800 °K equal to 61MPa.

According to what was said, to calculate the rate of transferred heat at the rotation of 500 rpm using Equation 1, we can write:

$$\dot{q}=\frac{4}{3}\pi^2\mu P\omega R^3=\frac{4}{3}\pi^2(0.36)\left(72\times10^6\text{Pa}\right)\left(\frac{500}{60}\text{rps}\right)\left(10\times10^{-3}\text{m}\right)^3=2842.45\text{W} \tag{2}$$

Also, to calculate the rate of transferred heat at the rotation of 710 rpm using Equation 1, we have:

$$\dot{q}=\frac{4}{3}\pi^2(0.36)\left(61\times10^6\text{Pa}\right)\left(\frac{710}{60}\text{rps}\right)\left(10\times10^{-3}\text{m}\right)^3=3419.62\text{W} \quad (3)$$

To consider boundary conditions, it is assumed that 10% of the heat created by the tool is wasted through the tool itself and the thermal conductivity [28]. Therefore, it is assumed that 90% of the heat created by the tool is spent to do the process. So, for the two mentioned states, the net heat transferred to the workpiece will be equal to:

At the rotation of 500 rpm:

$$\dot{q}_{net}=0.9\times2842.45\text{W}=2558.2\text{W} \quad (4)$$

and at the rotation of 710 rpm:

$$\dot{q}_{net}=0.9\times3419.62\text{W}=3077.65\text{W}. \quad (5)$$

It is also assumed that water with the ambient temperature passes through two channels of copper sheet and exchanges the heat through (convective) transmission with the copper sheet and therefore with the workpiece. All of the other cases of heat exchange during the process performance are negligible and were ignored; for example, the heat transferred by the workpiece to air or small components of the die.
If the specific heat capacity of water is considered as c = 4200 J/kg $^\circ$K [29] to obtain the outlet water temperature of the die, we can write:
At the rotation of 500 rpm:

$$\dot{q}_{net}=\dot{m}c\Delta T\Rightarrow2558.2\text{W}=0.019\frac{\text{kg}}{\text{s}}\times4200\frac{\text{J}}{\text{kg}^\circ\text{K}}\times\Delta T\Rightarrow\Delta T=32^\circ\text{K} \quad (6)$$

And at the rotation of 710 rpm:

$$3077.65\text{W}=0.019\frac{\text{kg}}{\text{s}}\times4200\frac{\text{J}}{\text{kg}^\circ\text{K}}\times\Delta T\Rightarrow\Delta T=38.6^\circ\text{K}. \quad (7)$$

The water temperature at the inlet to the die was 298 $^\circ$K. Therefore, the water temperature at the outlet will be 330 $^\circ$K at the rotation of 500 rpm and 336.6 $^\circ$K at the rotation of 710 rpm. To perform the simulation, the average temperature of the inlet and outlet has been considered as cooling water temperature i.e. temperatures of 314 $^\circ$K and 317.3 $^\circ$K for rotations 500 rpm and 710 rpm, respectively.
To calculate the convective heat transfer coefficient (h), the relation of convective heat transfer has been used:

$$\acute{q}=Ah\Delta T \quad (8)$$

In the Equation 8, $\acute{q}$ is the rate of heat transferred to the cooling water and A is the area of the die channel moistened by water (Figure 6), so we have:

$$A=2\times[(6+30+6)\times100]\text{mm}^2=8.4\times10^{-3}\text{m}^2 \quad (9)$$

Now, given that the heat that the copper sheet at the bottom of die takes from the workpiece is directly transferred to cooling water, we have:

$$\acute{q}=\dot{q}\Rightarrow Ah\Delta T=\dot{m}c\Delta T\Rightarrow h=\frac{\dot{m}c}{A}=\frac{0.019\frac{\text{kg}}{\text{s}}\times4200\frac{\text{J}}{\text{kg}^\circ\text{K}}}{8.4\times10^{-3}\text{m}^2}=9500\frac{\text{W}}{\text{m}^2\,^\circ\text{K}} \quad (10)$$

However, it should be noted that h coefficient is not often a constant value and depends on parameters such as the length of the pipe (channel) and Nusselt number, etc., but the value obtained from the above relation can be accepted as average h in the channel.

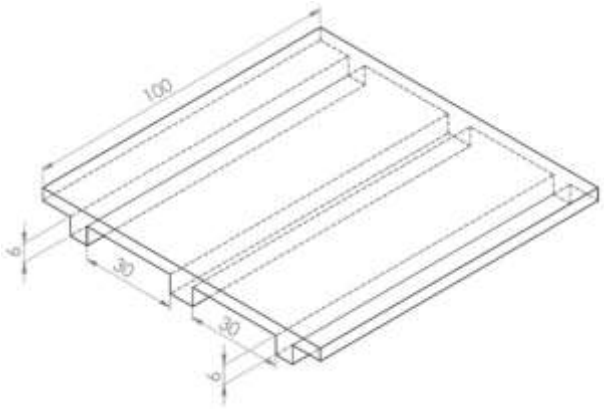


***Figure 6.*** *Dimensions of two die channels.*

Given that the specific heat capacity and thermal conductivity coefficient of copper have different values at various temperatures, these two quantities were introduced to software in terms of temperature, according to Table 3 [30].

***Table 3.*** *Specific heat capacity and thermal conductivity coefficient of copper at various temperatures [30].*

| Temperature (ºK) | Thermal conductivity (W/mºK) | Heat capacity (J/KgºK) |
|---|---|---|
| 200 | 412 | 343 |
| 350 | 396 | 391 |
| 500 | 387 | 403 |
| 650 | 376 | 425 |
| 800 | 365 | 437 |
| 950 | 355 | 455 |
| 1100 | 345 | 468 |
| 1250 | 334 | 478 |

For the more similarity of simulations to the conducted experiments, the thermal source has been considered as a fixed point of space and just above of the two half pieces and at the beginning of their intersection. Two half workpieces are passed completely similar to the test across their intersection, beneath and tangent to it and with constant speeds. Each half of workpiece has been meshed by 2700 cubic elements.

As it was explained in the section of experiments, two halves of the workpieces and the copper sheets of the bottom of die do significant heat exchange. So, this exchange should be considered in the simulation. Therefore, in addition to the two halves of workpiece, copper sheet of the die and its two water passing channels, have been modeled using 2800 cubic elements. Given that the workpiece became practically tight on the die copper by the die constraints and completely contacted with it at any moment, meshing of the workpieces and die copper was done in the way that nodes of their elements (in their contact plane) overlapped at each other. In the next step, the nodes consistent with each other were merged to desirably do the heat exchange between two halves of the workpieces and die copper. So, there is no need to define the contact between various components of the issue. In this simulation, due to its high accuracy, the model of piecewise linear plasticity material has been used since using this model, the parts of stress – strain diagram of the material are identically presented to the software without the need for the curve fitting. The copper density has been considered equal to $8900\frac{\text{kg}}{\text{m}^3}$ and the initial temperature of all components equal to 298 $^{\circ}$K.

## 4. RESULTS AND DISCUSSION

### 4.1. Thermal History and Field

Through simulations, the thermal field can easily be achieved at any time and for any welding mode. Figure 7 shows the thermal field in three different welding conditions and when welding tool is located in the middle of the weld line. Also, Figure 8(a) indicates the thermal history for the point of workpieces whose thermal history has experimentally been measured and Figure 8(b) reveals the thermal history for the point which the heat source passes and places in the middle of the weld line.

According to Figure 8, it is evident that the effect of rotational speed of tool on the maximum rate of temperature is much more than the effect of its traverse velocity. Figure 8(b) reveals that 100% increase in the traverse velocity from 56 mm/min to 112 mm/min has led to decrease the maximum temperature from 715 $^{\circ}$K to 693 $^{\circ}$K which is by no means a significant value. On the other hand, if the rotational speed increases from 500rpm to 710rpm that is 24% rises, the maximum temperature will increase from 715 $^{\circ}$K to 802 $^{\circ}$K. Also, according to diagrams of Figure 8 although, increasing in traverse velocity hasn't a significant effect on the thermal history of different points of the workpiece, it causes to decrease the duration of welding time i.e. transferring less heat to the workpiece. Moreover, Figure 8(a) shows that with increasing the rotational speed of the tool, the interested point of workpiece bear more temperature and an increasing in the temperature is significant. Therefore, in summary, it can be said that the traverse velocity change mainly affects the transferred heat rate and the change in the rotational speed dramatically change the temperature of the process.

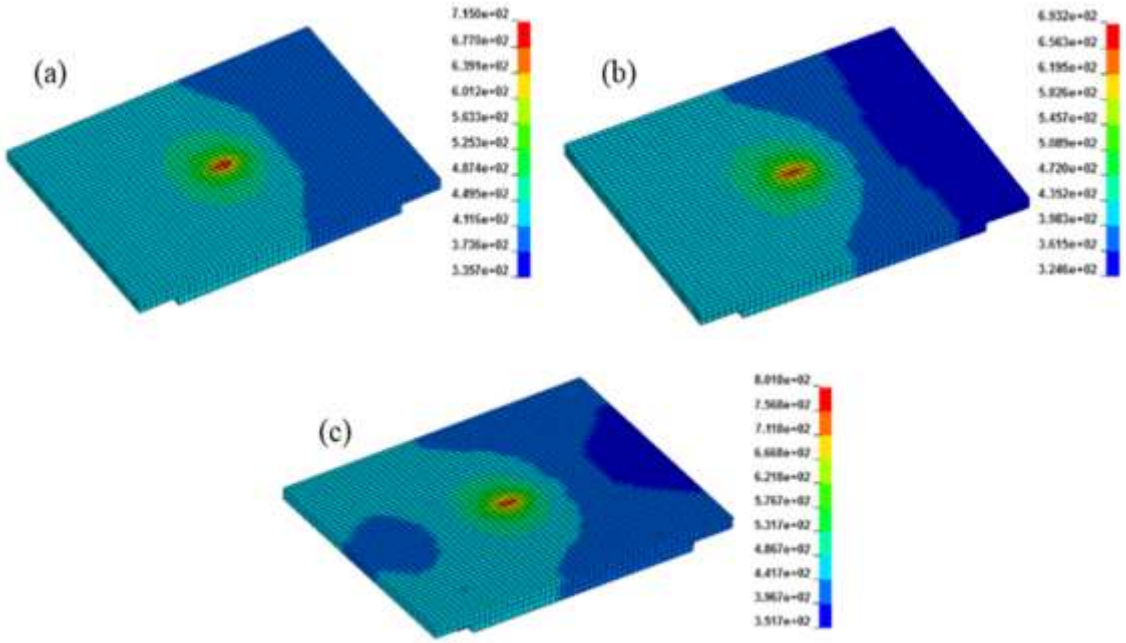


***Figure 7.*** *Temperature field in three different welding conditions (according to Table 2) of welding: (a) welding conditions 1, (b) welding conditions 2 and (c) welding conditions 3.*

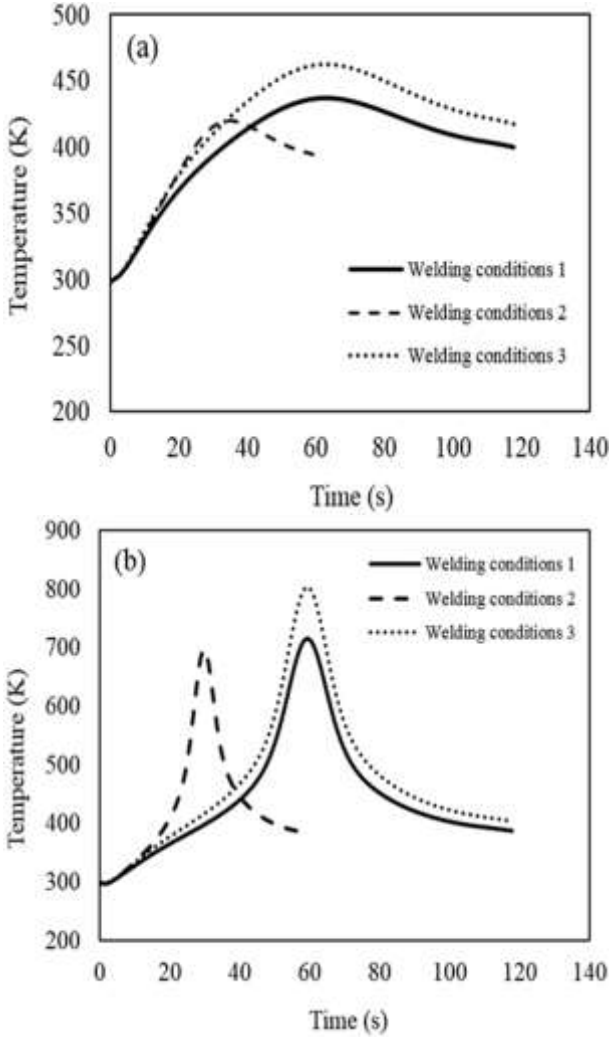


***Figure 8.*** *(a) The thermal history in the point of workpieces whose thermal history has experimentally been measured and (b) the thermal history in the point on which the heat source passes and places in the middle of the intersection line of two pieces.*

In order to compare the experimental and numerical results, the diagrams of the thermal history of each method have been obtained for various welding conditions mentioned in Table 2, are shown in Figure 9. According to these diagrams, it can be found that at first, the simulation diagrams are lower than the diagrams obtained from the experiment because the estimated heat rate is slightly less than the true heat rate. This is because in estimating the heat rate, flow stress has been considered equal to the flow stress of the horizontal part of the diagram; while, the overall flow stress is slightly higher than this value. However, in large strains which occur in the friction stir process, this part of the diagram is not quite noticeable. Afterward, the trend of process diagrams reverses and the simulation diagrams place higher than the experiment diagrams, that is because of the effect of ignored heat loss. Over time, their values in experiment increase while, there is no loss in the simulation. But it should be noted that the values of these differences are not significant compared to temperatures on which the process is done and with a little ignorance, the obtained diagrams can be considered to be coincide.

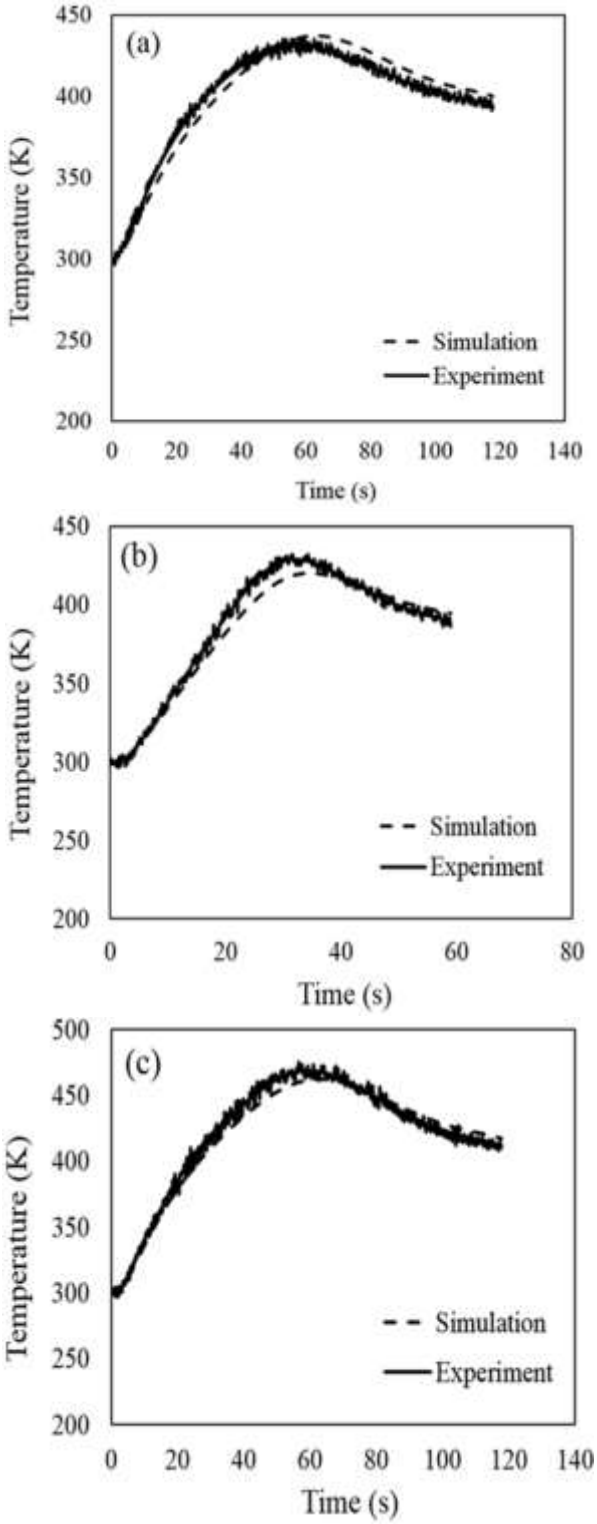


***Figure 9.*** *Comparing the experimental and simulation results (a) Welding conditions 1; (b) Welding conditions 2 and (c) Welding conditions 3.*

This matter demonstrates that the thermal history and field can be predicted by doing a tension test on samples prepared from the intended material and using LS-Dyna software and its thermal weld option. So, it is clear that using the advantages of the numerical method, many time and cost can be saved and the thermal history and field at any moment in workpieces such as complex pieces can be predicted correctly no need to practical weld.

In addition, this study shows that the relation proposed by Frigadd et al. has been successful to estimate the rate of heat transferred to the workpiece within FSW and thus, the relation is valid for the copper workpiece.

### 4.2. Thermal Stresses Optimization

Thermal stress line profiles from the upper-plate thickness are provided in Figure 10 for the FSW sample sets produced with different welding conditions. Figure 10(a) shows the longitudinal thermal stresses profiles and Figure 10(b) shows the transversal thermal stresses profiles. The gold of this study is the minimization of thermal stresses because thermal stresses are the main reason of created residual stresses in the welded plates. Residual stresses are an important issue in FSW, particularly in fatigue loading because, large tensile residual stresses can be produced during welding processes which can lead to premature fatigue failure. So, the tensile residual stresses should be minimized. For this purpose, it is essential to understand how the welding parameters influence the thermal stress distribution.

Taguchi method is one of the popular optimization techniques that could be used to optimize welding parameters. Optimization of process parameters is a key step in the Taguchi technique to reach high quality without increasing the cost. This is because optimization of FSW process parameters can decrease the tensile thermal stress (TTS), which leads to improvement of performance characteristics [21].

Generally, classical process parameter design is complex and not easy to solve. This is mainly true when the number of the process parameters increases, leading to a large number of simulations have to be carried out. To solve this problem, the Taguchi method with a special design of orthogonal arrays can be employed to study the entire process parameter space with a small number of simulations only. The optimum combination of the process parameters can then be predicted.

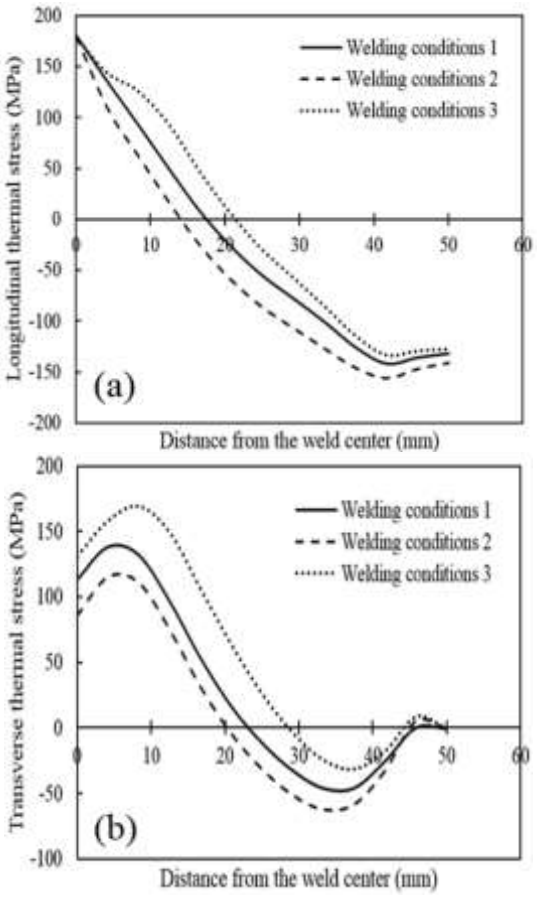


***Figure 10.*** *(a) Predicted longitudinal thermal stresses profiles and (b) Predicted transversal thermal stresses profiles for a half of welded copper plates under different welding conditions.*

As mentioned, the goal of this section is the optimization of thermal stresses produced by the FSW process on copper sheets using simulation method. By using the Taguchi method, the DOE is employed to optimize welding parameters including rotational speed and traverse velocity of tool and shoulder diameter.

The process parameters are considered in five levels each as shown in Table 4. In order to minimize the number of simulations, Taguchi's $L_{25}$ factorial design of simulation was adopted in this work, the design matrix is given in Table 5.

***Table 4.*** *Process parameters at five levels.*

| parameters | Level 1 | Level 2 | Level 3 | Level 4 | Level 5 |
|---|---|---|---|---|---|
| Rotational speed (rpm) | 500 | 552 | 605 | 657 | 710 |
| Traverse speed (mm/min) | 56 | 70 | 84 | 98 | 112 |
| Tool shoulder (mm) | 20 | 21 | 22 | 23 | 24 |

***Table 5.*** *Taguchi's $L_{25}$ design matrix.*

| Sim. No. | Rotational speed (rpm) | Traverse speed (mm/min) | Tool shoulder (mm) |
|---|---|---|---|
| 1 | 500 | 56 | 20 |
| 2 | 500 | 70 | 21 |
| 3 | 500 | 84 | 22 |
| 4 | 500 | 98 | 23 |
| 5 | 552 | 112 | 24 |
| 6 | 552 | 56 | 21 |
| 7 | 552 | 70 | 22 |
| 8 | 552 | 84 | 23 |
| 9 | 552 | 98 | 24 |
| 10 | 552 | 112 | 20 |
| 11 | 605 | 56 | 22 |
| 12 | 605 | 70 | 23 |
| 13 | 605 | 84 | 24 |
| 14 | 605 | 98 | 20 |
| 15 | 605 | 112 | 21 |
| 16 | 657 | 56 | 23 |
| 17 | 657 | 70 | 24 |
| 18 | 657 | 84 | 20 |
| 19 | 657 | 98 | 21 |
| 20 | 657 | 112 | 22 |
| 21 | 710 | 56 | 24 |
| 22 | 710 | 70 | 20 |
| 23 | 710 | 84 | 21 |
| 24 | 710 | 98 | 22 |
| 25 | 710 | 112 | 23 |

It is clear that owing to process parameters changes, the transferred heat rate to the sheets changes and therefore, the temperature of coolant water, induced residual stresses and flow stress of workpiece change. So, for every welding cases, these quantities should be determined using the corresponding formula and numerical method. For determination of transferred heat rate to the sheets in all 25 welding conditions mentioned in Table 5, Equation (1) was used.

Simulation results show that the amounts of longitudinal thermal stresses are more than the amounts of traverse residual stresses. Other researchers have obtained the same conclusion [31, 32]. In addition, the maximum of longitudinal tensile thermal stresses has occurred on the weld line. Thus, in this study, the maximum of longitudinal TTS which is created on the weld line is considered as an objective function that is the most longitudinal tensile thermal stress. Table 6 presents the transferred heat rate to the sheets,

the flow stress, the temperature of water at the outlet and the induced longitudinal TTS for 25 considered welding conditions in Table 5.

***Table 6****. Transferred heat rate to the sheets, the flow stress, the temperature of water at the outlet and the induced longitudinal TTS for 25 considered welding conditions in Table 5.*

| Sim. No. | Transferred heat rate (W) | Flow stress (MPa) | temperature of water at outlet (ºK) | longitudinal TTS (MPa) |
|---|---|---|---|---|
| 1 | 2842.45 | 72.00 | 330.00 | 142.05 |
| 2 | 3081.83 | 67.43 | 332.76 | 143.01 |
| 3 | 3312.17 | 63.04 | 335.35 | 139.68 |
| 4 | 3532.80 | 58.84 | 337.84 | 136.92 |
| 5 | 3742.16 | 54.85 | 340.20 | 134.22 |
| 6 | 3245.30 | 64.32 | 334.60 | 147.72 |
| 7 | 3476.11 | 59.92 | 337.20 | 134.88 |
| 8 | 3694.91 | 55.75 | 339.67 | 131.57 |
| 9 | 3901.71 | 51.81 | 342.00 | 128.60 |
| 10 | 3003.64 | 68.92 | 331.87 | 149.10 |
| 11 | 3627.02 | 57.05 | 338.91 | 130.37 |
| 12 | 3844.03 | 52.92 | 341.35 | 126.53 |
| 13 | 4047.15 | 49.03 | 343.64 | 123.52 |
| 14 | 3154.90 | 66.04 | 333.58 | 144.40 |
| 15 | 3397.02 | 61.43 | 336.31 | 141.46 |
| 16 | 3976.00 | 50.39 | 342.84 | 122.47 |
| 17 | 4175.93 | 46.58 | 345.09 | 118.77 |
| 18 | 3291.25 | 63.44 | 335.12 | 140.06 |
| 19 | 3533.48 | 58.83 | 337.85 | 136.91 |
| 20 | 3761.66 | 54.48 | 340.42 | 133.85 |
| 21 | 4294.29 | 44.33 | 346.43 | 114.61 |
| 22 | 3419.62 | 61.00 | 336.56 | 136.21 |
| 23 | 3660.59 | 56.41 | 339.28 | 132.16 |
| 24 | 3886.95 | 52.09 | 341.84 | 129.04 |
| 25 | 4098.19 | 48.07 | 344.22 | 126.21 |

Table 6 shows that the minimum of TTS is 114.61 and belongs to welding conditions 21. In welding conditions 21, the rotational speed is 710rpm, traverse speed is 56mm/min and tool shoulder is 24mm. in this welding conditions, the maximum heat transfers to the workpiece. So, the welding conditions 21 is the optimal welding conditions, of course from the point of view of the minimum longitudinal TTS. It should be noted that in welding conditions 21, the amount of the maximum of TTS is optimal (minimum) respect to other welding conditions that is because of thermal softening that means the more the heat transferred to the workpiece, the less the pick of induced thermal stress. Of course, if the objective of optimization was the optimizing of longitudinal TTS in the whole of the workpiece, the welding conditions that transferred the least heat to the workpiece (welding conditions 1) was the best.

In the present study, thermal stress had been investigated as the main parameter in order to achieve a joint with minimum longitudinal TTS. In order to better analysis, signal to noise analysis was used to minimize longitudinal TTS values. Since the objective of this study is to maximize longitudinal TTS through optimum process parameters in friction stir welding, “Smaller is better” quality characteristic is applied in this study. For this purpose, the S/N ratio is calculated using the below formula:

$$\frac{S}{N} = -10Log\left(\frac{1}{n}\sum_{i=1}^{n} Y_i^2\right) \tag{11}$$

Where $Y_i$ is the value of longitudinal TTS for the *i*th simulation, *n* is the number of simulations and *N* is the total number of data points.

According to Table 6, 25 main values for longitudinal TTS and 25 corresponding values of S/N were obtained. The optimal combination of factors and levels were obtained by analyzing each calculated main values, in order to achieve the minimum longitudinal TTS. As it is clear, higher values of S/N ratio of a simulation, corresponds to the better quality of the welded joint. Therefore the optimal condition is a condition with the maximum S/N ratio. Values of S/N ratio of longitudinal TTS in different levels of used parameters are shown in Figure 11. The analyses are made using the popular software known as MINITAB 16.

As Figure 11shows, value of longitudinal TTS is minimum when rotational speed, traverse speed and shoulder diameter were in 710rpm, 56mm/min and 24mm levels respectively, because, values of S/N ratios in these levels are maximum. Also, to determine that which FSW process parameters have the maximum effect on the longitudinal TTS, it is needed to investigate the S/N ratio. Figure 11 gives a clear picture as to how far the process parameter affects the longitudinal TTS and the level of significance of each factor involved in the analysis. In fact, the main effects for S/N ratio are plotted in Figure 11. The high S/N ratio value indicates that the factor is highly significant in affecting the response of the process. In this investigation, shoulder diameter is a highly significant factor and plays a major role in affecting the longitudinal TTS.

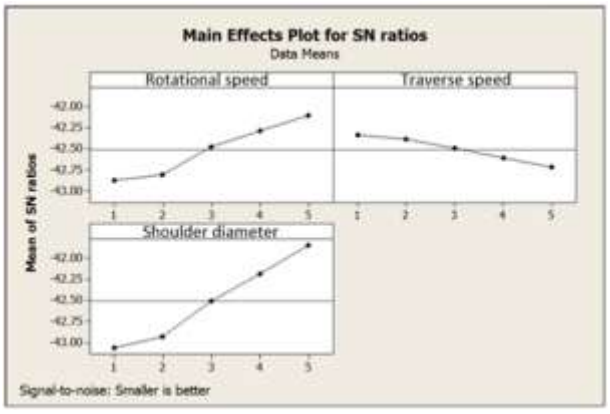


***Figure 11.*** *Values of S/N ratio of longitudinal TTS in different levels of used parameters.*

## 5. CONCLUSIONS

In this study, the thermal histories in copper sheets were determined experimentally and numerically during a Friction Stir Welding butt joining process and were compared with each other. The following conclusions can be drawn based on the results:

1- The traverse velocity change mainly affects the transferred heat rate and the change in the rotational speed dramatically changes the temperature of the process. For example 100% increase in the traverse velocity from 56 to 112mm/min has led to decrease in the maximum temperature from 715 to 693°K which is by no means a significant value, while the rotational speed increasing from 500 to 710 rpm, accordingly 24-percent rise, increases the maximum temperature from 715 to 802°K.
2- The relation proposed by Frigadd et al. has been estimated successfully the rate of heat transferred to the workpiece within FSW, thus the relations valid for the copper workpiece.
3- In all welding conditions, at first, the simulation diagrams are lower than the diagrams obtained from the experiment because the estimated heat rate is slightly less than the true heat rate. Afterward, the trend of process diagrams reverses and the simulation diagrams place higher than the experiment diagrams, that is because of the effect of ignored heat loss occurred in the experiment.
4- Signal-to-noise analysis shows that shoulder diameter is a significant factor and plays a major role in affecting the longitudinal tensile thermal stresses.

## CONFLICT OF INTEREST

No conflict of interest was declared by the authors

## REFERANCES

[1] Oztoprak, N., Yeni, C.E. and Kiral, B.G., "Fatigue and monotonic tensile behaviors of friction stir welded AA6061/SiC/20p-T1 composite joints at various tool rotation speeds" *Mater. Res. Express* 5, 066547 (2018).

[2] Khalkhali, A., Ebrahimi-Nejad, S. and Malek, N.G., "Comprehensive optimization of friction stir weld parameters of lap joint AA1100 plates using artificial neural networks and modified NSGA-II" *Mater. Res. Express* 5, 066508 (2018).

[3] Pirizadeh. M., Azdast, T., Rash Ahmadi, S., Mamaghani Shishavan, S. and Bagheri, A., "Friction stir welding of thermoplastics using a newly designed tool" *Mater. & Des*., 54, 342-347, (2014).

[4] Khalilpourazarya, S., Behnagha, R., A., Mahdavinejadb, R. and Payama, N., "Dissimilar friction stir lap welding of Al-Mg to CuZn34: Application of grey relational analysis for optimizing process parameters" *J. Comput. Appl. Res. Mech. Eng*., 4, 81-88, (2014).

[5] Cao, X.J. and Jahazi, M., "Friction stir welding of dissimilar AA 2024-T3 to AZ31B-H24 alloys" *Materials Science Forum: Trans Tech Publ*, 46, 3661-3666, (2010).

[6] Zhao, Y., Jiang, S., Yang, S., Lu, Z. and Yan, K., "Influence of cooling conditions on joint properties and microstructures of aluminum and magnesium dissimilar alloys by friction stir welding" *Int. J. Adv. Manuf. Technol*, 83, 673-679, (2016).

[7] Nia, A.A. and Shirazi, A.," Effects of different friction stir welding conditions on the microstructure and mechanical properties of copper plates" *Int. J. Miner. Metal. Mater*, 23, 799-809, (2016).

[8] Kumar, H., Khan, M.Z., and Vashista, M. "Microstructure, mechanical and electrical characterization of zirconia reinforced copper based surface composite by friction stir processing" *Mater. Res. Express* 5, 086505 (2018).

[9] Sun, Y.F. and Fujii, H., "Investigation of the welding parameter dependent microstructure and mechanical properties of friction stir welded pure copper" *Mater. Sci. Eng. A*, 527, 6879-6886, (2010).

[10] Khodaverdizadeh, H., Mahmoudi, A., Heidarzadeh, A., and Nazari, E., "Effect of friction stir welding (FSW) parameters on strain hardening behavior of pure copper joints" *Mater. Des.*, 35, 330-334, (2012).

[11] Shi, P., Wang, Q., Xu, Y. and Luo, W., "Corrosion behavior of bulk nanocrystalline copper in ammonia solution" *Mater. Letters*, 65, 857-859, (2011).

[12] Pehkonen, S.O., Palit, A. and Zhang, X., "Effect of specific water quality parameters on copper corrosion" *Corros*, 58: 156-165, (2002).

[13] Shim, J.J., and Kim, J.G., "Copper corrosion in potable water distribution systems: influence of copper products on the corrosion behavior" *Mater. Letters*: 58, 2002-2006, (2004).

[14] Boulay, N. and Edwards, M., "Role of temperature, chlorine, and organic matter in copper corrosion by-product release in soft water" *Water res*., 35, 683-690, (2001).

[15] Hwang, Y.M., Kang, Z.W., Chiou, Y.C. and Hsu, H.H., "Experimental study on temperature distributions within the workpiece during friction stir welding of aluminum alloys" *Int. J. Mach. Too. Manuf.*, 48, 778-787, (2008).

[16] Xue, P., Xiao, B.L., Zhang, Q. and Ma, Z.Y., "Achieving friction stir welded pure copper joints with nearly equal strength to the parent metal via additional rapid cooling" *Scripta Mater*., 64, 1051-1054, (2011).

[17] Imam, M., Biswas, K. and Racherla, V., "On use of weld zone temperatures for online monitoring of weld quality in friction stir welding of naturally aged aluminium alloys" *Mater. Des*., 52, 730-739, (2013).

[18] Buffa, G., Ducato, A., and Fratini, L., "Numerical procedure for residual stresses prediction in friction stir welding" *Finit. Elem. in Anal. Des*., 47, 470-476, (2011).

[19] Jacquin, D., De Meester, B., Simar, A., Deloison, D., Montheillet, F. and Desrayaud, C., "A simple Eulerian thermomechanical modeling of friction stir welding" *J. Mat. Process. Technol*., 211, 57-65, (2011).

[20] Al-Badour, F., Merah, N., Shuaib, A., and Bazoune, A., "Coupled Eulerian Lagrangian finite element modeling of friction stir welding processes" *J. Mater. Process. Technol*., 213, 1433-1439, (2013).

[21] Javadi, Y., Sadeghi, S. and Najafabadi, M.A., "Taguchi optimization and ultrasonic measurement of residual stresses in the friction stir welding" *Mater. Des*., 55, 27-34, (2014).

[22] Ugender, S., "Influence of tool pin profile and rotational speed on the formation of friction stir welding zone in AZ31 magnesium alloy" J. *Magnesium Alloy*., 6, 205-213, (2018).

[23] Alavi Nia, A. and Shirazi, A., "An investigation into the effect of welding parameters on fatigue crack growth rate and fracture toughness in friction stir welded copper sheets" *Proc. Ins. Mech. Eng. Part L: J. Mater. Des. Appl.*, 232, 191-203, (2015).

[24] Zhao. Y., Wang, Q., Chen, H., and Yan, K., "Microstructure and mechanical properties of spray formed 7055 aluminum alloy by underwater friction stir welding" *Mater. Des*., 56, 725-730, (2014).

[25] Vigh, L.G., and Okura, I., "Fatigue behaviour of Friction Stir Welded aluminium bridge deck segment" *Mater. Des*., 44, 119-127, (2013).

[26] ASTM E8-16a "Standard Test Methods for Tension Testing of Metallic Materials: ASTM International" (2009).

[27] Mishra, R.S. and Ma, Z.Y., "Friction stir welding and processing" *Mater. Sci. Eng. R* 50 1-78 (2005).

[28] Blau, P.J., "Friction science and technology: from concepts to applications" CRC press (2008).

[29] Incropera, F.P., DeWitt, D.P., Bergman, T.L. and Lavine, A.S., "Foundations of heat transfer" *Wiley Textbooks* (2012).

[30] Jin, L.Z. and Sandstrom, R., "Numerical simulation of residual stresses for friction stir welds in copper canisters*" J. Manuf. Process*, 14, 71-81, (2012).

[31] Sun, T., Roy, M.J., Strong, D., Withers, P.J. and Prangnell, P.B., "Comparison of residual stress distributions in conventional and stationary shoulder high-strength aluminum alloy friction stir welds" *J. Mater. Process. Technol.*, 242, 92-100, (2017).

[32] Zapata, J., Toro, M. and Lopez, D., "Residual stresses in friction stir dissimilar welding of aluminum alloys" *J. Mater. Process. Technol*., 229, 121-127, (2016).

GU J Sci, Part A, 6(1): 25-32 (2019)

Gazi University

**Journal of Science**

PART A: ENGINEERING AND INNOVATION

http://dergipark.gov.tr/gujsa

# Optimization of Surface Roughness in Turning of AZ31 Magnesium Alloys with Taguchi Method

Ömer ASAL[1,*]

[1]*Gazi Üniversitesi, Teknoloji Fakültesi, İmalat Mühendisliği Bölümü, Beşevler, Ankara*

**Article Info**

*Research Article*
*Received: 20/03/2019*
*Accepted: 28/03/2019*

**Keywords**

*Turning,*
*AZ31,*
*Taguchi method,*
*ANOVA,*
*Surface roughness*

**Abstract**

In this paper, the effects of the different cutting parameters on the surface roughness in turning AZ31 magnesium alloys were investigated. Three cutting parameters, such as depth of cut (t), feed rate (f) and cutting speed (V), were used in the turning operation. Experiments were designed for L9 Taguchi's model. Tests were performed on a CNC lathe. The surface roughness values were measured in the tests. Taguchi and ANOVA analysis were evaluated to detect main effect parameters and their contribution ratios. The optimum cutting parameters for the surface roughness were computed as "t" at level 2 (2 mm), "f" at level 1 (0.2 mm/rev) and "V" at level 1 (320 m/min). Moreover, empirical equations were developed by using regression analysis (RA) to predict the surface roughness and compared to experimental results.

## 1. INTRODUCTION

Magnesium alloys have been widely used in automobile, electronics, and aerospace fields. Magnesium alloys are a promising material for attractive features that will replace aluminum and steel in structural and mechanical applications. They have a superior hardness-to-weight ratio, a high damping capacity, the lowest density among engineered metallic materials and the ease of recyclability [1]. At present, magnesium alloys are used for many applications due to their light weight instead of aluminum alloys [2,3]. Although near net shape manufacture of magnesium alloy parts is possible through various die casting techniques, more often than not machining steps will still need to be carried out on such parts. Researchers applied some optimization techniques to improve machining quality of the magnesium alloys in the literature. Sahu and Pal [3] investigated of the optimization of process parameters in friction stir welded AM20 magnesium alloy by Taguchi grey relational analysis. Tönshoff and Winkler investigated influence of tool coatings on the machining of magnesium. They found that TiN and PCD coated tools reduce cutting force, and result in improved surface quality even at high cutting speeds [4]. Shi et al., performed surface roughness and micro hardness in dry milling of magnesium alloy using Taguchi with grey relational analysis [5]. The optimum parameters for better surface quality in turning Mg-Ca3.0 alloy were investigated by Denkena and Lucas [6]. Umbrello [7] investigated of surface integrity in dry machining of Inconel 718. Jin and Liu [8] performed Effect of cutting speed on surface integrity and chip morphology in high-speed machining of PM nickel-based super alloy FGH95. Pu et al. have investigated the influence of tools with varying cutting edge radii on magnesium surfaces under dry and cryogenic machining conditions [9].

In this study, the effects of the various cutting parameters that are the depth of cut (t), the feed rate (f) and the cutting speed (V) on the surface roughness of the AZ31 magnesium alloy materials in turning process were identified by using Taguchi method. The highest contribution ratios of each parameter of the surface

*Corresponding author, e-mail: omerasal@gazi.edu.tr

roughness were performed by ANOVA analysis. Moreover, empirical equations was evaluated with regression analysis (RA) for the surface roughness and compared with experimental results.

## 2. MATERIAL AND METHOD

Experimental tests were performed in a CNC lathe under dry machining conditions. The work pieces of the experimental tests were used high-pressure die-cast AZ31 magnesium alloy bar with 92 mm diameter and 300 mm length. The test part was manufactured as Fig. 1 to do the experiments and controls easily.

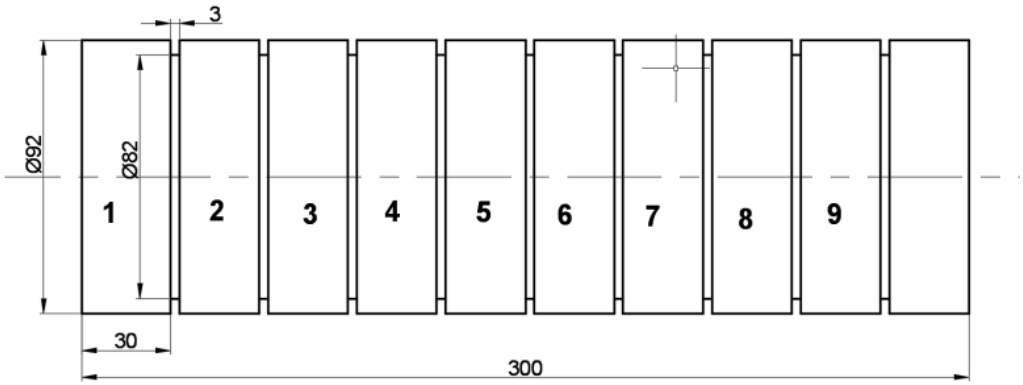


***Figure 1***. *Test part*

The chemical composition of the AZ31 material was presented in Table 1

***Table 1***. *The chemical composition (%) of AZ31 magnesium alloy.*

| Al | Zn | Mn | Fe | Si | Cu | Ni | Mg |
|---|---|---|---|---|---|---|---|
| 3.23 | 0.84 | 0.21 | 0.0032 | 0.014 | 0.0014 | 0.00042 | Balance |

The cutting tools coated PVD (SNMG120412-NM4 WSM10) were used in the machining process. Mahr Perthometer M1 type, given specifications (Table 2), was used as surface roughness measurement instrument. The surface roughness of the AZ31 alloy was measured with the measurement instrument.

***Table 2.*** *Specifications of the surface roughness measurement instrument*

| | |
|---|---|
| Tracing speed | 0.5 m/sn |
| Tracing force | 0.75 mN |
| Stylus radius | 2 μm |
| Sampling range | 100 – 150 μm |
| Profile | 12 mm |
| Filter | Gaussian |
| Sampling | 0.25 – 0.8 – 2.5 (mm) |
| Measurement | 1.75 – 5.6 – 17.5 (mm) |
| Roughness | Ra, Rz, Rmax |

Three different cutting parameters, such as depth of cut, feed rate, and cutting speed (Table 3), were used for machining AZ31 alloy.

***Table 3.*** *The cutting parameters used in the machining AZ31 Magnesium Alloy*

| Symbol | Machining Parameter | Coded levels | | |
|---|---|---|---|---|
| | | 1 | 2 | 3 |
| A | Depth of cut, t (mm) | 1 | 2 | 3 |
| B | Feed rate, f (mm/rev) | 0.1 | 0.2 | 0.3 |
| C | Cutting Speed, Vc (m/min) | 320 | 512 | 820 |

## 3. RESULTS AND DISCUSSION

Normally, (3 x 3 x 3) 27 experiments are required for all machining parameters' levels (Table 3) in classical machining test. It is seen that the experiments mean time and cost. It is known that Taguchi method is preferred to conduct the experiments. Taguchi also is called design of experimental method that provide with minimum experiments to identify main effects of the using parameters in tests [10,11]. So in this paper, the effect of the cutting parameters on the surface roughness was investigated by using Taguchi method. Taguchi method was done to test AZ31 magnesium alloy in MINITAB. The control factors and each parameter used for experimental design were presented in Table 3. The numbers of experiments were reduced by the using of Taguchi method. The numbers of experiments were found enough as 9 by Taguchi in machining AZ31 magnesium alloy. In this way, the experimental works were designed as L9 (3*3) orthogonal array in Taguchi method. Taguchi L9 design of experiments model was given in Table 4.a.

Tests were fulfilled on a CNC Lathe according to Taguchi L9 model. The surface roughness (Ra) was measured for each of the test. Totally, 9 experiments were performed, two repeated. The tests results were given in Table 4.b.

It is known that the minimum surface roughness is very important criteria in machining methods, such as turning, milling, drilling. Moreover, there are a lot of factors that affect the surface roughness in machining methods, for example, federate, cutting edge radius, depth of cut, etc. Therefore, the results of the tests were analyzed to determine the main effects on surface roughness by using the analysis of Taguchi Design in MINITAB. The S/N ratio was used to analyze test results of the machining AZ31 magnesium alloy. The S/N ratio that is a method in the analysis of Taguchi Design was performed to evaluate the test results. There are several functions, such as, "*Lager is better"*, "*Nominal is best"* and *"Smaller is better",* to analyze test results with Taguchi method.

In this experimental works, the main function that is the "*Smaller is better"* quality characteristics was preferred to determine the optimal cutting parameters for surface roughness. "*Smaller is better"* quality characteristics of the signal-to-noise (S/N) ratio was given as below:

$$\eta = -10\log\left(\frac{1}{n}\sum_{i=1}^{n} y_i^2\right) \tag{1}$$

***Table 4****. a) Experimental design for the $L_9$ orthogonal array, b) The tests results*

| Exp. No | A | B | C |
|---|---|---|---|
| 1 | 1 | 1 | 1 |
| 2 | 1 | 2 | 2 |
| 3 | 1 | 3 | 3 |
| 4 | 2 | 1 | 2 |
| 5 | 2 | 2 | 3 |
| 6 | 2 | 3 | 1 |
| 7 | 3 | 1 | 3 |
| 8 | 3 | 2 | 1 |
| 9 | 3 | 3 | 2 |

a)

| Exp. No | A (t: mm) | B (f: mm/min) | C (V: m/min) | Ra (µm) |
|---|---|---|---|---|
| 1 | 1 | 0.1 | 320 | 0.416 |
| 2 | 1 | 0.2 | 512 | 1.496 |
| 3 | 1 | 0.3 | 820 | 2.533 |
| 4 | 2 | 0.1 | 512 | 0.518 |
| 5 | 2 | 0.2 | 820 | 1.027 |
| 6 | 2 | 0.3 | 320 | 2.532 |
| 7 | 3 | 0.1 | 820 | 0.631 |
| 8 | 3 | 0.2 | 320 | 1.157 |
| 9 | 3 | 0.3 | 512 | 3.029 |

b)

Where $\eta$ is the S/N ratio for the "*Smaller is better"* case, and $y_i$ represents the surface roughness based on experimental results and *n* the number of repetitions in a trial [11-17]. Table 5 present the S/N ratio obtained from Eq. (1) for surface roughness. The effect of each factor at different levels can be determined by averaging the S/N ratios. To determine the "*Smaller is better"* surface roughness quality, the S/N ratio applied at each level of each factor (Table 5). The main effective factors and order shows in the Rank column. The numbers point order of the main factors out. The Rank numbers are obtained from the values of Delta column. If the Delta value is bigger than other the Rank value will be first number (1). So, the first main factor is B (feed rate) according to the number 1 of the Rank column. In other words, the parameter feed rate is the main factor for the surface roughness in turning AZ31 magnesium alloy.

***Table 5.*** *Response table mean S/N ratio (η) for Ra (μ) (smaller is better)*

| Symbol | Parameter | Mean S/N ratio, η | | | | |
|---|---|---|---|---|---|---|
| | | **Level 1** | **Level 2** | **Level 3** | **Delta** | **Rank** |
| A | Cutting depth, t (mm) | -1.3177 | -0.8624 | -2.2977 | 1.4353 | 3 |
| B | Feed rate, f (mm/rev) | 5.7770 | -1.6656 | -8.5893 | 14.3663 | 1 |
| C | Cutting Speed, V (m/min) | -0.5726 | -2.4704 | -1.4349 | 1.8978 | 2 |

Also, the obtained results were presented in an S/N response graphical form as shown in Fig. 2. The trend of the curves in Fig. 2 shows the effects of the test factors. In other words, the shape of curves that are formed by the levels of factors tells us which factors are very or less important for test results. For example, the feed rate curve in Fig. 2 rises quickly. As a result, the feed rate is absolutely main factor for surface roughness of AZ31 magnesium alloy.

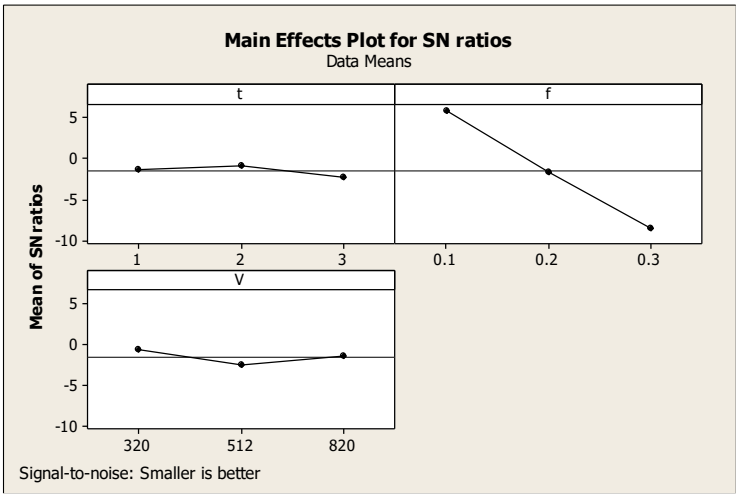


***Figure 2.*** *Mean S/N ratio graph for surface roughness, Ra (μ)*

ANOVA was performed to investigate the effect the design parameters on quality characteristics [16]. The percent contribution ratio (PCR) was determined for surface roughness using ANOVA. The PCR to determine of influence of cutting parameters was computed from Eq. (2) [13-17]:

$$PCR = \left( \frac{SS_A - (V_e).(\upsilon_A)}{SS_T} \right) \times 100 \tag{2}$$

Where $SS_A$, is the sum of squares for parameter A. $V_e$ is the variance of error, $\upsilon_A$ is the degrees of freedom of parameter A, and $SS_T$ is the total sum of squares [18-19]. In addition, the effect of the cutting parameters on the surface roughness in turning process was evaluated by using ANOVA as regards PCR. As shown in Table 6, feed rates were found to be the major factor affecting the surface roughness (PCR:

94.18%) followed by cutting speed (PCR: 0.10 %). However, the depth of cut has no effect on surface roughness.

***Table 6.*** *ANOVA results for surface roughness, Ra (μm) (for S/N ratios)*

| **Source** | **Degrees of freedom (DoF)** | **Sequential sum of squares (SS)** | **Mean sum of squares (MS)** | **F-test** | **P-coefficient** | **PCR (%)** |
|---|---|---|---|---|---|---|
| Depth of cut | 2 | 3.228 | 1.614 | 0.63 | 0.612 | --- |
| Feed rate | 2 | 309.721 | 154.860 | 60.77 | 0.016 | 94.18 |
| Cutting speed | 2 | 5.417 | 2.709 | 1.06 | 0.485 | 0.10 |
| Residual error | 2 | 5.096 | 2.548 | | | 5.72 |
| Total | 8 | 323.462 | | | | 100 |

In Table 7, the optimum cutting parameters were determined with *S*/*N* ratio by using the Taguchi method. The optimal cutting parameter for the best surface roughness with the criteria of the lowest response and lowest S/N ratio was obtained as A2B1C1 (Table 5). Also, the figure 1 appears the effects levels of the factors that make the surface roughness minimum. The depth of cut at level 2 (2 mm), feed rate at level 1 (0.1 mm/rev) and cutting speed at level 1 (320 m/min) provided the best results for optimum cutting parameters as regards surface roughness [20]. But, these parameters are not include L9 Taguchi model (Table 4). The A2B1C1 values that are t: 2 mm, f: 0.1 mm/rev. and v: 320 m/min., were not used in the experimental works. So, the levels were untested. For this reason, Taguchi method provides to predict the untested levels of factors. The predicted surface roughness for A2B1C1 was evaluated by Taguchi method. Moreover, a confirmation test was carried out for making certain of these parameters [18]. The having gotten results were presented in Table 7.

***Table 7.*** *Results of confirmation tests for surface roughness, Ra (μm)*

| | **Optimal cutting parameters** | |
|---|---|---|
| | **Prediction** | **Experimental** |
| Level | A2B1C1 | A2B1C1 |
| Surface roughness, Ra (μm) | 7.32723 | 0.515 |
| Mean S/N ratio | 0.284778 | 5.7638 |

An equation can be computed for the predictive surface roughness. So, the regression analysis should be used by evaluating an equation. It is known that the regression analysis correlates among the used test parameters and find the coefficients for using in the equation [20]. In this paper, the regression analysis for the surface roughness equations obtained by using MINITAB software. The Coefficients for surface equations were given in Table 8.

***Table 8****. Regression analysis results for surface roughness, Ra (μm*)

| **Predictor** | **Coef** | **SE Coef** | **T** | **P** |
|---|---|---|---|---|
| Constant | -0.7993 | 0.5073 | -1.58 | 0.176 |
| t | 0.0620 | 0.1384 | 0.45 | 0.673 |
| f | 10.882 | 1.384 | 7.86 | 0.001 |
| V | -0.0000343 | 0.0005488 | -0.06 | 0.953 |

S = 0.339074 R-Sq = 92.5% R-Sq(adj) = 88.1%

The reliability for the Regression analysis was computed by 92.5%. Moreover, if the coefficients in table 8 are used, the equation will be obtained as follow.

$$Ra = - 0.7993 + 0.0602\ t + 10.882\ f – 0.0000343\ V \quad (3)$$

In addition, Analysis of Variance for regression was evaluated in Table 9. In Table 9, the value of the P is 0.003 that shows accuracy of the ANOVA analysis. Also, the value shows the acceptability results of the analysis. Because, it is lower than 0.005 that is 95% confidence.

***Table 9.*** *Regression analysis results for surface roughness, Ra (µm)*

| Source | **DF** | **SS** | **MS** | **F** | **P** |
|---|---|---|---|---|---|
| Regression | 3 | 7.1282 | 2.3761 | 20.67 | 0.003 |
| Residual Error | 5 | 0.5749 | 0.1150 | | |
| Total | 8 | 7.7030 | | | |

In addition, the four residual plots for Ra by Regression method were presented in Fig. 3. The plots can give an idea for the Regression analysis.

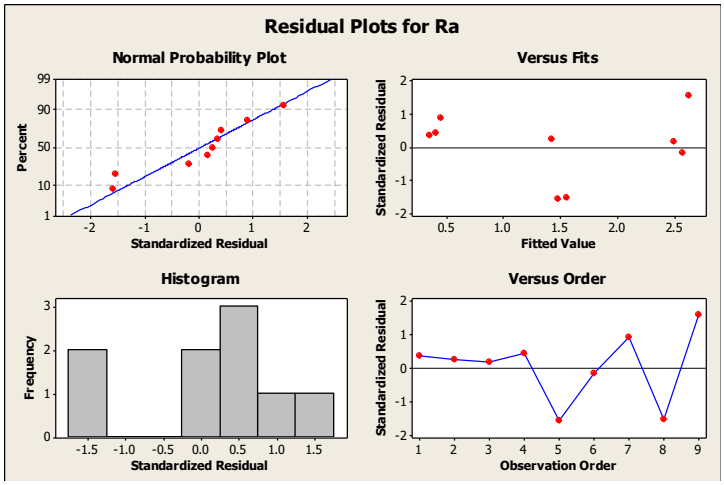


***Figure 3.*** *The four residual plots for Ra by Regression method*

Finally, new results for Ra were found by using the regression equation (3). The obtained values are shown in Table 10. The percent error values evaluated from are shown a little bit high in Table 10. It is thought that the values are a reason of the L9 Taguchi model. The Taguchi L9 model limited for evaluating the regression analysis to predict the test results properly. If the large Taguchi model could be selected for example, L27, The regression predicted results would be more close the experiments results.

***Table 10.*** *The tested results and the Regression equation results for surface roughness, Ra (µm)*

| **Ra (µm) Experimental** | **Ra (µm) Regression Equation** | **Error (%)** |
|---|---|---|
| 0.416 | 0.34212 | 17.7596 |
| 1.496 | 1.42559 | 4.7066 |
| 2.533 | 2.50512 | 1.1007 |
| 0.518 | 0.39759 | 23.2452 |
| 1.027 | 1.47712 | 43.8286 |
| 2.532 | 2.58412 | 2.0585 |
| 0.631 | 0.44912 | 28.8241 |
| 1.157 | 1.55612 | 34.4961 |
| 3.029 | 2.63959 | 12.8561 |

## 4. CONCLUSIONS

In this paper, the surface roughness of turning process for various cutting parameters, such as depth of cut, the feed rate and the cutting speed, were optimized by using Taguchi Method. The results can be listed as:

- The optimum cutting parameters for the lowest surface roughness were found as A2B1C1 with the depth of cut at level 2 (2 mm), feed rate at level 1 (0.1 mm/rev) and cutting speed at level 1 (320 m/min).
- The most significant factor affecting the surface roughness was determined to be the feed rates (94.14 %) followed by the cutting speed (PCR: 0.10 %). However, the depth of cut has no effect on surface roughness.
- The empirical equations were developed and confirmation test were applied. The results obtained between experimental and predicted results have indicated a good agreement within the ranges of the applied cutting parameters.
- The large Taguchi model should be selected in the experimental works if a regression analysis is done.

## CONFLICT OF INTEREST

No conflict of interest was declared by the authors

## REFERANCES

[1] Zeng, R.C., Chen, J., Dietzel, W., Zettler, R., Santos, J.F.D., Nascimento, M.L., Kainer, K.U., "Corrosion of friction stir welded magnesium alloy AM50", *Corrosion Science*, 51 (2009), 1738-1746. https://doi.org/10.1016/j.corsci.2009.04.031

[2] Dhanapal, A., Boopathy, S.R., Balasubramanian, V., "Corrosion behaviour of friction stir welded AZ61A magnesium alloy welds immersed in NaCl solutions", *Transactions of Nonferrous Metals Society of China*, 22 (2012), 793-802. https://doi.org/10.1016/S1003-6326(11)61247-8

[3] Prakash K.S., Sukhomay P., "Multi-response optimization of process parameters in friction stir welded AM20 magnesium alloy by Taguchi grey relational analysis", *Journal of Magnesium and Alloys* 3 (2015), 36-46. https://doi.org/10.1016/j.jma.2014.12.002

[4] Tönshoff, H.K., Winkler, J., "The influence of tool coatings in machining of magnesium", *Surface & Coatings Technology*, 94-95 (1997), 610-616. https://doi.org/10.1016/S0257-8972(97)00505-7

[5] Kaining S., Dinghua Z., Junxue R., "Optimization of process parameters for surface roughness and microhardness in dry milling of magnesium alloy using Taguchi with grey relational analysis", *Int. J. Adv. Manuf. Technol*., 81 (2015), 645-651 DOI 10.1007/s00170-015-7218-8

[6] Denkena, B., Lucas, A., "Biocompatible magnesium alloys as absorbable implant materials-adjusted surface and subsurface properties by machining processes", *CIRP Ann Manuf. Technol*. 56 (2007), 113-116. https://doi.org/10.1016/j.cirp.2007.05.029

[7] Umbrello, D., "Investigation of surface integrity in dry machining of Inconel 718", *Int. J. Adv. Manuf. Technol,*. 69 (2013), 2183-2190. DOI 10.1007/s00170-013-5198-0

[8] Jin, D., Liu, Z., "Effect of cutting speed on surface integrity and chip morphology in high-speed machining of PM nickel-based superalloy FGH95", *Int. J. Adv. Manuf. Technol*., 60 (2011), 893-899. DOI 10.1007/s00170-011-3679-6

[9] Pu, Z., Outeiro, J.C., Batista, A.C., Dillon, Jr. O.W., Puleo, D.A., Jawahir, I.S., "Surface Integrity in Dry and Cryogenic Machining of AZ31B Mg Alloy with Varying Cutting Edge Radius Tools", 1st *CIRP Conference on Surface Integrity (CSI), Procedia Engineering,* 19 (2011) 282-287. https://doi.org/10.1016/j.proeng.2011.11.113

[10] Taguchi G., ElSayed E. A., and Hsiang T. C., "Quality Engineering in Production Systems", *McGraw–Hill*, New York, NY, USA, (1989).

[11] Ross P.J., "Taguchi Techniques for Quality Engineering", 2nd ed., *McGraw-Hill*, New York, USA, (1996).

[12] Zhang J. Z., Chen, J.C., and Kirby, E.D., "Surface roughness optimization in an end-milling operation using the Taguchi design method", *Journal of Materials Processing Technology* 184 (2007), 233-239. https://doi.org/10.1016/j.jmatprotec.2006.11.029

[13] Çakıroğlu, R., Acır, A., "Optimization of cutting parameters on drill bit temperature in drilling by Taguchi method", Measurement 46 (2013), 3525-3531. https://doi.org/10.1016/j.measurement.2013.06.046

[14] Yang, W.H., and Tarng, Y.S., "Design optimization of cutting parameters for turning operations based on the Taguchi method", *Journal of Materials Processing Technology,* 84 (1998), 122-129. https://doi.org/10.1016/S0924-0136(98)00079-X

[15] Acır, A., Canlı, M.E., Ata, I., Çakıroğlu, R., "Parametric optimization of energy and exergy analyses of a novel solar air heater with grey relational analysis", *Applied Thermal Engineering*, 122 (2017), 330-338. https://doi.org/10.1016/j.applthermaleng.2017.05.018

[16] Çakıroğlu, R., Acır, A., "Taguchi optimization method of tool chip interface temperature depending on the cutting parameters in drilling operations", *Makine Teknolojileri Elektronik Dergisi*, 10 (2013), 73-86

[17] Baysal, E., Bilginsoy, A.K., Acır, A., "Parametric optimization on exergy analysis of a thermal power plant using Taguchi Method", *Energy Education Science and Technology Part A-Energy Science and Research*, 29 (2012), 1313-1326.

[18] Kayir Y. "Optimization of the Cutting parameters for Drilling Magnesium Alloy AZ 91", *Materials Testing*, 56(1), (2014), 47-53.

[19] Yalçin N., Kayir Y., Erkal S. "Investigation of Effects of The Aging Methods Applied on AA2024 Aluminium Alloys on Machinability With Taguchi and ANOVA", *Journal of Polytechnic*, 20, (2017), 743-751., Doi: 10.2339/politeknik.368552

[20] Sarikaya, M., Yilmaz, V., Dilipak, H., "Modeling and multi-response optimization of milling characteristics based on Taguchi and gray relational analysis", *Proc. Inst. Mech. Eng. Part B-J. Eng. Manuf.*, 230 (June) (2016), pp. 1049-1065. https://doi.org/10.1177/0954405414565136